Corrosion performance and mechanical properties of FeCrSiNb amorphous equiatomic HEA thin film

Waleed Muftah* John Allport and Vladimir Vishnyakov

Centre for Engineering materials, University of Huddersfield, HD1 3DH, UK

Abstract

A quaternary amorphous equiatomic FeCrSiNb HEA thin film was synthesised and characterised with the view for applications in demanding environments. The film was produced on silica and silicon substrates by ion beam sputter deposition. Scanning Electron Microscopy (SEM) was used to analyse the film morphology, and Energy-dispersive X-ray spectroscopy (EDX) was used to investigate the atomic composition. The crystal structure of the sample was investigated using X-Ray Diffraction (XRD) and Selected Area Electron Diffraction (SAED). The film is amorphous and uniform at the atomic level. An electrochemical cell with a three-electrode arrangement was utilized to assess the corrosion behaviour of the sample in 0.6 M NaCl and H_2SO_4 solutions at room temperature under ambient pressure. In addition, the corrosion tests were conducted in a Libyan crude oil to simulate an oil field corrosion process. The corrosion results showed that the FeCrSiNb HEA thin film has an excellent corrosion resistance, and that the corrosion resistance is much better than that of 304 SS in 0.6 M NaCl, H_2SO_4 solutions, and in crude oil. The amorphous equiatomic FeCrSiNb HEA thin film has high hardness at around 15 ± 1.2 GPa, and reduced Young's modulus at around 229 ± 12 GPa.

Keywords:

FeCrSiNb equiatomic alloy, amorphous, high entropy alloy HEA, thin film, corrosion resistance, hardness and reduced Young's modulus.

*) Corresponding author: Waleed Muftah, Waleed.Muftah@hud.ac.uk

1. Introduction:

In a comparison with crystalline alloys, amorphous or metallic glasses alloys do not have grain boundaries with disordered atomic-scale structure. Therefore, amorphous alloys show a higher wear resistance, fatigue strength and better corrosion resistance than crystalline alloys in many cases according to certain compositions [1-3]. This high performance of amorphous alloys has attracted scientists and engineers to use them in applications in the shipbuilding and petroleum industries [4], and in biomedical devices [5]. However, amorphous alloys as conventional alloys comprise two, three or more elements based on one or two main elements such as Cu-based [6] and Zr-based [7]. They, also exhibit defects in some cases [8].

To break the classical alloy-design philosophy, a new class of materials have been discovered. High entropy alloys (HEAs) contain five or more elements in equiatomic or near equiatomic ratios to form a simple single-phase structure [9-11]. The entropy effect increases with the increase of the number of elements added to the composition, [12] as well as with the equiatomic ratio that ranged between 5 and 35 atomic percent of every single element [13, 14]. High entropy alloy studies usually seem to be motivated by the concept that high configurational entropy might favour a uniform single-phase structure with intermetallic phases [14]. However, many studies state that HEAs can have less than five elements with atomic concentration more than 35 and less than 5 in some case. This leads to the same or closer effect that can be found in the equiatomic high entropy alloys [15-23]. These type of alloys are known as compositionally concentrated alloys [24, 25], and/or complex concentrated alloys (CCAs) [26-28].

Generally, HEA alloys are crystalline and tend to form a single-phase structure comprising one of the following structures: face-centred cubic (FCC), body-centred cubic (BCC) or hexagonal close-packed (HCP), with homogenous structure in a few cases such as $Fe_{20}Cr_{20}Mn_{20}Ni_{20}Co_{20}$ [11], and $Fe_{20}Cr_{20}Mn_{20}Ni_{20}C_{20}$ which was investigated in earlier work [29]. However, the

majority have multi-phase structure with elemental separation for example; $Fe_{50}Mn_{30}Co_{10}Cr_{10}$ [30], $FeCoNiAl_{0.2}Si_{0.2}$ [31], and $Ta_{20}Nb_{20}Hf_{20}Zr_{20}Ti_{20}$ [32].

Furthermore, HEAs also can be amorphous where they are known as amorphous high entropy alloys or bulk metallic high entropy alloys BM-HEAs, which are defined as alloys composed four or more elements with equimolar concentration rapid quenched from the vapour or liquid state such as: $Ti_{20}Zr_{20}Cu_{20}Ni_{20}Be_{20}$ [33], $Ca_{20}Mg_{20}Zn_{20}Sr_{20}Yb_{20}$ [34], and $Fe_{25}Co_{25}Ni_{25}(B, Si)_{25}$ [35]. These types of alloys are found to satisfy the target properties in required applications, for instance to have high corrosion resistance where the absence of grain boundaries could lead to improve the corrosion resistance of the alloy [36]. More information can be found within the following citation [37]. This new type of alloys could help to avoid the defects (voids and element segregation) that found in the conventional amorphous alloys where the limited number of principle elements restricts material potential development [4]. This point was further confirmed and discussed in our previous study on an equiatomic FeCrMnNiC thin films [38].

High Entropy Alloys in general possess enhanced structural stability as compared to majority of conventional alloys owing to the mixing of high entropy effect, lattice distortion effect, sluggish-diffusion effect which attributed to the limited rate of diffusion as Yeh has firstly described it [9]. Due to the presence of five or more principal elements in the solid solution phases with no dominant element in the compositions, the effective diffusion rate will be restricted because of the lattice distortion which provides additional energy barriers to atom movement. The diffusion kinetics of high entropy alloys is slower than in conventional alloys. Therefore, HEAs possess larger stability in the structure than conventional alloys [39-41]. The effect of stabilised mixing of few elements in equiatomic ratios leads to greater and unpredictable results. The combination of lattice distortion due to differences in elements atomic sizes, impeded diffusion, and high entropy all lead to new combined effects, so named “cocktail effects” [42].

Combination of unique structure and properties in HEAs have attracted significant attention and made HEAs to be key candidates for several engineering areas [43, 44]. For example, the alloys can be used in applications requiring high thermal stability [45-47], high hardness [48-51], high strength and ductility [30, 52, 53], excellent irradiation stability [54-56], good wear resistance [57, 58], good resistance to fatigue [59-61] and high oxidation resistance [62-64].

From a corrosion point of view, a considerable number of studies have been conducted to determine the corrosion behaviour of high entropy alloys in different solutions such as NaCl, H_2SO_4 and HCL at room temperature and under atmospheric pressure, and HEAs exhibited better corrosion resistance than stain less steel [65-68]. The first such experiment was done by Hsu et al in 2005. The study was conducted on varying the amount of copper on FeCoNiCrCu high entropy alloy in 3.5 % NaCl solution using a potentiodynamic polarization technique. The results showed that an increasing of the Cu content led to elemental segregation, thus decreasing the corrosion resistance. Also the uniform alloy exhibited the best corrosion resistance [69]. Moreover, the effect of Al amount on $Al_xCoCrFeNi$ HEA showed the same result in which the resistance to corrosion reduced as the structure changed from a single phase to two phases in a 0.5 M H_2SO_4 solution. [70]. Similarly, an increase in the amount of Mn led to reduction in the corrosion resistance of $Al_{0.3}CoCrFeNiMn_x$ in 3.5 % NaCl solution [71]. However, there are some exceptions, for instance the increase in Mo content was beneficial and enhancing the pitting corrosion on $Co_{1.5}CrFeNi_{1.5}Ti_{0.5}Mo_x$ in 1M NaCl solution [72]. It could therefore be inferred that a uniform and homogeneous alloy structure could lead to better corrosion resistance of HEA alloys [73].

Recently, surface coating techniques have been considered as an additional advantage to increase the corrosion resistance of HEAs. From the economic standpoint, the costs of high entropy bulk alloys prepared by vacuum arc melting furnace or casting are relatively high. However, coatings could solve this problem by making the overall cost lower [74]. Additionally, a HEA coating with the same composition as a bulk HEA displayed better

corrosion resistance, which could be referred to more homogeneous and uniform structure and also to the thickness of the coating [75]. As a consequence, HEA coatings, including thin films, have been successfully deposited on different substrates by several methods and demonstrated excellent corrosion resistance. This has been shown for thin film alloys synthesised by magnetron sputtering [76-80], laser cladding [66, 81], plasma spraying [82], plasma cladding [83] and mechanical alloying method [84].

In the oil and gas field, the most commonly used alloys are based on chromium and/or nickel content as they provide a good protective passive layer to protect the surface from corrosion. However, this passive layer is only effective up to a certain point and time in the presence of harsh environments such as CO_2 and H_2S. By breaking down the passive layer, the material surface becomes weak and susceptible to corrosion where pitting starts to occur. This leads to a failure of the material surface, which is a big problem for petroleum applications. [85-87]. In this paper we aim to provide a solution to this problem. A FeCrSiNb equiatomic amorphous HEA thin film was prepared by ion beam sputter deposition. The microstructure was investigated by set of techniques. Corrosion testing was performed using NaCl and H_2SO_4 solutions, and crude oil. Also, mechanical properties were examined.

2. Materials and methods:

Ion beam sputter deposition system was used to synthesise and deposit the thin film alloy on silicon (100 orientated wafers) and optically polished silica substrates. The overall deposition process was fully outlined in earlier work [88, 89]. Silicon wafers were cleaved into 1 square inch pieces and then carefully dusted with lint-free cloth and compressed air. The silica glass, 1 square inch pieces, was used as delivered from the manufacturer without additional cleaning.

The elements chosen for this work were Fe, Cr, Si and Nb in sheet shapes. The positions of the targets were adjusted several times towards the substrate to achieve the equiatomic

composition. The deposition was conducted under stable parameters of current, pressure and temperature. The base system pressure was $2.2 * 10^{-4}$ Pa, and the Argon partial pressure in the deposition chamber during the deposition system was about $3.3 * 10^{-2}$ Pa. The deposition was done at room temperature aiming to achieve the amorphous structure. In the deposition chamber, the targets were cleaning via the plasma for around 30 minutes before starting the deposition on the substrate. This is to avoid sputtering any contaminations might be left on the targets surface while substrate exchanges. The thickness of the thin film after around 120 minutes was measured by the FIB (focused ion beam) sectioning method to be approximately 1.5 microns.

For microstructural observation, a FEI Quanta FEG250 Scanning Electron Microscope (SEM) was used to study the thin film surface. Energy-dispersive X-ray spectroscopy (EDX) using an Oxford Instruments was employed to determine the chemical composition. The crystal structure of the film was investigated using X-Ray Diffraction (XRD) on a Bruker D2 Phaser instrument and Measurement Center 4.0 software. In addition, a Transmission Electron Microscope (TEM, Hitachi-9500.) sample was made by Focused Ion Beam (FIB), and Selected Area Diffraction (SAD) was utilised to examine the atomic structure in thoroughly. 300 keV electron beam was used for TEM analysis.

Corrosion tests were performed using potentiodynamic polarization technique in a three-electrode cell setup. The specimens, deposited on silicon, were set up as working electrodes (with an exposed area of 0.5 cm^2), with a platinum counter electrode and using saturated calomel electrode as the reference. The tests were carried out in 0.6 M NaCl and H_2SO_4 solutions. Both solutions were purged with nitrogen in order to remove dissolved oxygen. In addition, the test was performed in a Libyan crude oil. The measurements were performed at room temperature and under atmospheric pressure. The potential and current were measured by means of an Autolab potentiostat fitted with Nova 1.10 software. According to ASTM International (American Society for Testing and Materials) standards, the scanning rate of each

test was set at 1 mV/s. Open Circuit Potential (OCP) measurements were performed for around half an hour (30 min) to achieve a stable potential. Polarization measurements were scanned between -0.1V and 1.2V. Corrosion parameters which are: corrosion potential (E_{corr}), corrosion current density (i_{corr}), and passivation regions were obtained by linear fit technique of polarization curves. For a comparison, stainless steel type 304 samples were used under same conditions.

For measuring mechanical properties of the amorphous equiatomic FeCrSiNb HEA thin film deposited on silicon, hardness and modulus were determined by a Nanoindentation system from Micro Materials Ltd, UK. A Berkovich nano-indenter was utilised to apply a ramped load up to maximum value of 50 mN.

3. Results and discussion:

3.1 Microstructure:

Figure 1 presents the data for a FeCrSiNb thin film synthesised by ion beam deposing system. A Backscatter Electron (BSE) image was taken at high magnification and is shown in fig.1 (a). The main purpose of BSE image is to clarify whether the elements are distributed uniformly or if there is any elemental and/or phase separation which will appear as contrast variation. In this case, the BSE image confirms that the microstructure of FeCrSiNb thin film is homogeneous and uniform. The Energy-dispersive X-ray spectroscopy (EDX) quantification showed that the alloy has an equiatomic composition as evident on Fig.1 (b).

(a)

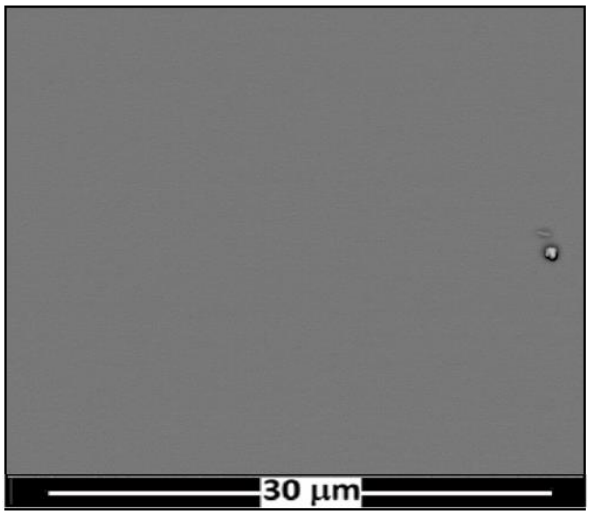

(b)

Element	Weight%	Atomic%
Si K	12.50	24.56
Cr K	24.67	26.18
Fe K	25.47	25.17
Nb L	40.56	24.09
Totals	100.00	

Figure 1: SEM analysis of the amorphous equiatomic FeCrSiNb high entropy alloy thin film. (a): BSE image microstructure image. (b): chemical composition of HEA thin film.

Element mapping of the FeCrSiNb thin film is presented on Fig.2. As it can be seen from the mapping, all the elements are distributed uniformly and homogeneously.

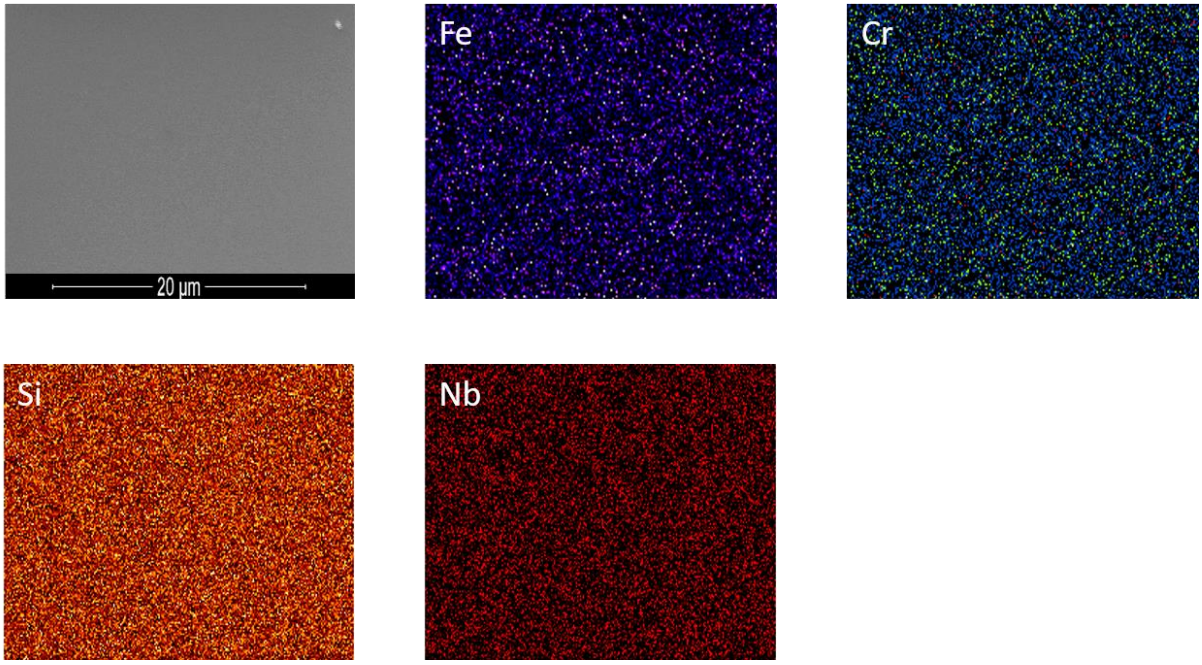

Figure 2: EDX mapping of the amorphous equiatomic FeCrSiNb HEA thin film.

In order to confirm the absence of element segregation, EFTEM (Energy filtered TEM) imaging of FeCrSiNb thin film was performed. The elemental maps prove a uniform distribution for all elements (iron, chromium, silicon and niobium) without any element segregation or precipitation as presented as on Fig. 3.

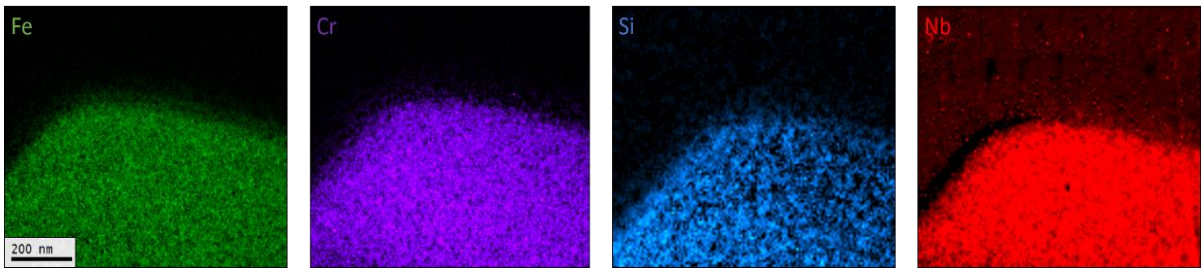

Figure 3: EFTEM images of the amorphous equiatomic FeCrSiNb HEA thin film.

In order to assess the film crystalline structure, the film was deposited on silica glass. The X-Ray diffraction pattern (XRD) demonstrates that the FeCrSiNb HEA thin film possesses no crystalline structure. The XRD pattern is characteristic to an amorphous material as displayed in Fig.4. The main film diffraction peak at around 44˚ is very broad and has low intensity which a typical amorphous material XRD. The second peak at 21˚ is related to the silica substrate as confirmed on Fig.5.

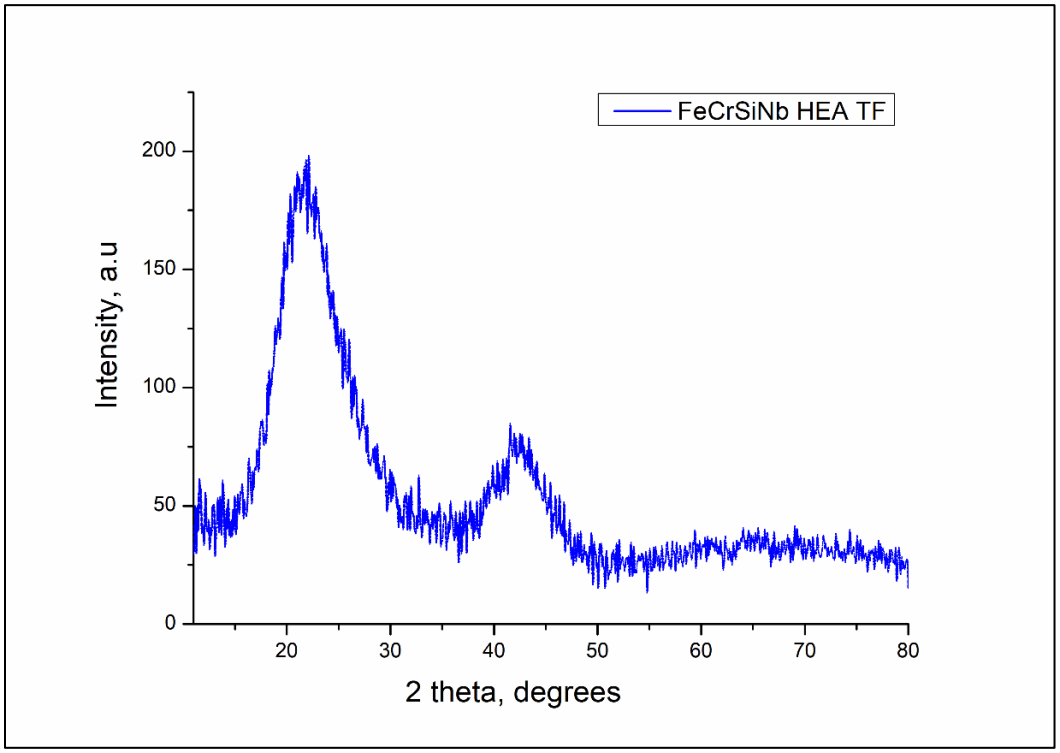

Figure 4: XRD pattern of the FeCrSiNb thin film on silica substrate.

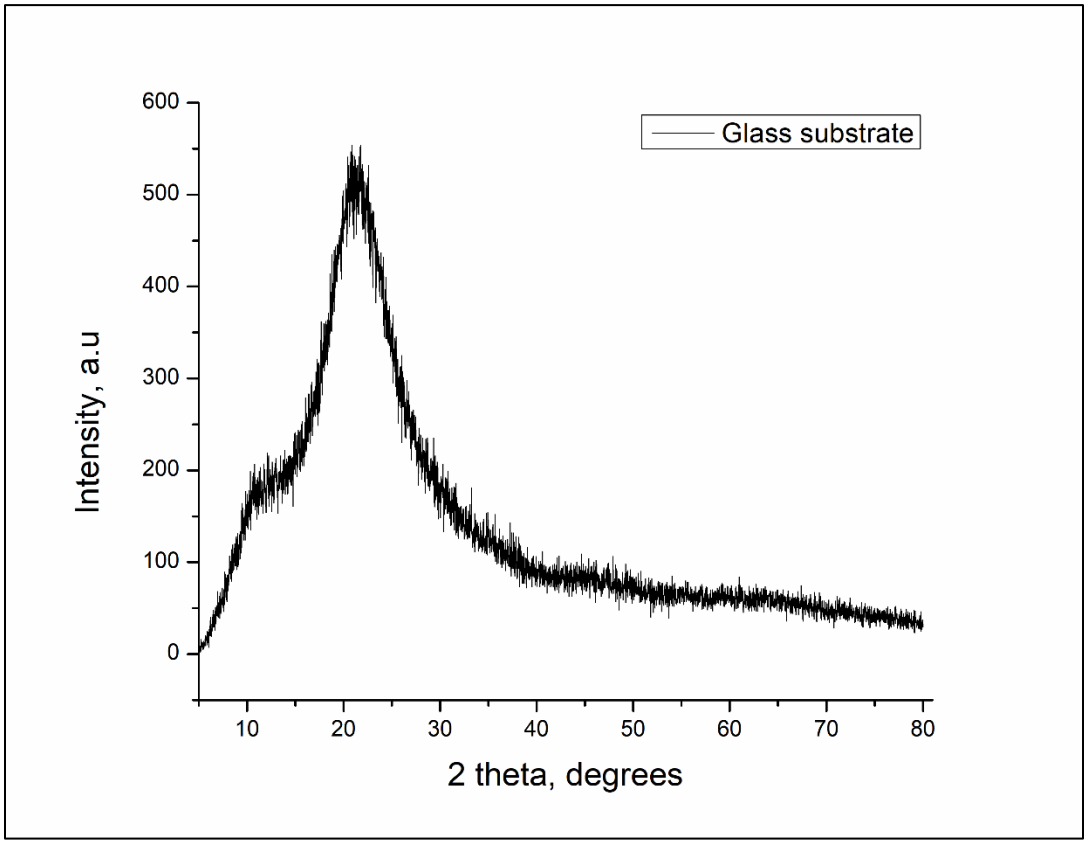

Figure 5: XRD pattern of the silica glass substrate.

For further examination of the amorphous structure of the amorphous equiatomic FeCrSiNb high entropy alloy thin film, a FIB (Focused Ion Beam) sample was studied in a Transmission Electron Microscope (TEM). Fig.6 (a) shows a bright field image (BFTEM) high-resolution TEM image of a high entropy thin film synthesised by ion beam sputtering. Fig.6 (b) is the selected area diffraction (SAED) of the thin film which was taken from the marked area, and confirms the formation of a fully amorphous structure by the presence of only diffraction rings without any crystallinity patterns.

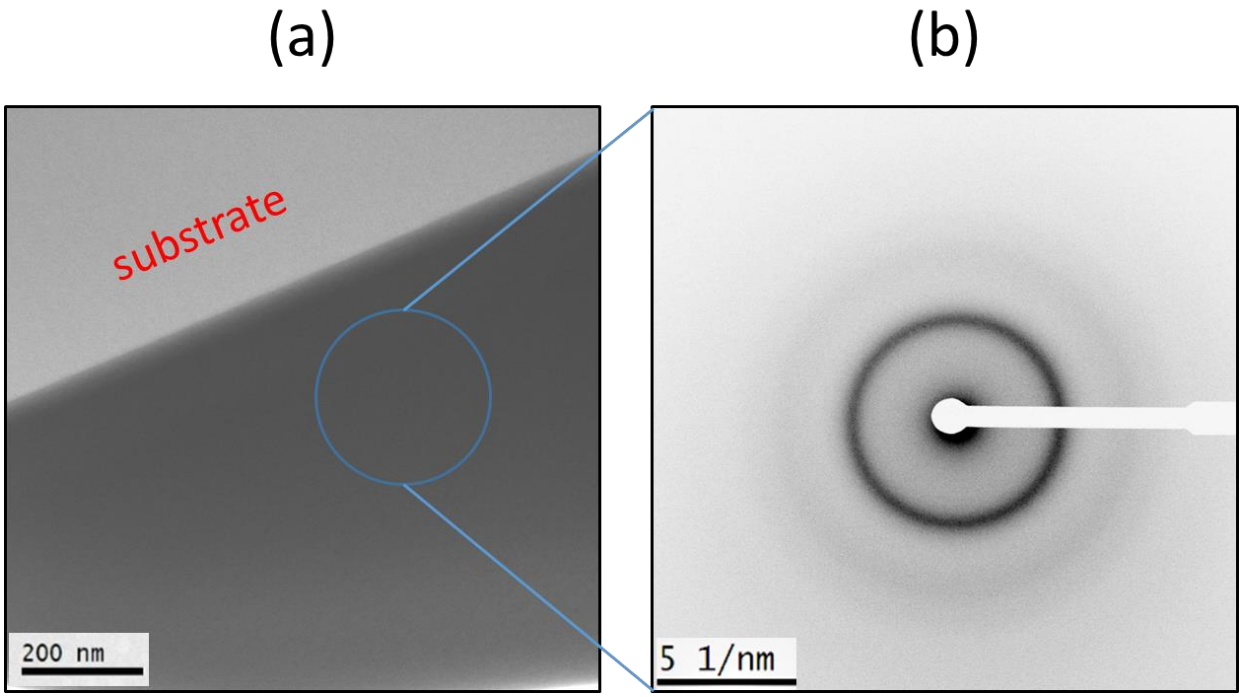

Figure 6 (a): BFTEM images of the amorphous equiatomic FeCrSiNb high entropy alloy thin film synthesised by ion beam sputtering, and fig. 6 (b) SAED images of amorphous film taken from marked area.

All the aforementioned results from the SEM-BSE, EDX mapping show that the amorphous equiatomic FeCrSiNb high entropy alloy thin film synthesised by ion beam sputter deposition

is a single phase and uniform alloy. This is mainly attributed to the layer-by-layer deposition which has been carried out under stable conditions of temperature and pressure [88, 89]. The formation of a dense and amorphous alloy has been confirmed by XRD and TEM results. The main reason for this is due to the transformation from ionic state to solid state which led to significantly high cooling rate at deposition chamber, and the condensation energy is released [90]. The amorphization of high entropy thin films could be attributed to the high mixing entropy and large atomic size difference. The high mixing entropy increases the mutual solubility of different elements in thin films and impedes the formation of phase separation [91]. Also, the presence of Niobium has played a vital role in improving amorphization process of the alloy. A study of the phase evolution in NbCoCrCuFeNi thin film deposited by magnetron sputtering has demonstrated that the film structure changed from a crystalline to an amorphous structure with a higher Nb content [92].

3.2 Corrosion tests:

Figure 7 shows a potentiodynamic polarisation curve of the amorphous equiatomic FeCrSiNb high entropy alloy thin film which was carried out in the three-electrode electrochemical cell in 0.6 M NaCl (3.5 % sodium chloride) solution under conditions of atmospheric pressure and room temperature. Table 1 presents corrosion parameters for FeCrSiNb HEA thin film which were obtained by a linear fit technique. Figure 8 is a potentiodynamic polarisation curve of the amorphous equiatomic FeCrSiNb HEA thin film which was conducted in in 0.6 M H_2SO_4 (sulphuric acid) solution under the same conditions. The obtained corrosion parameters are listed in table 2.

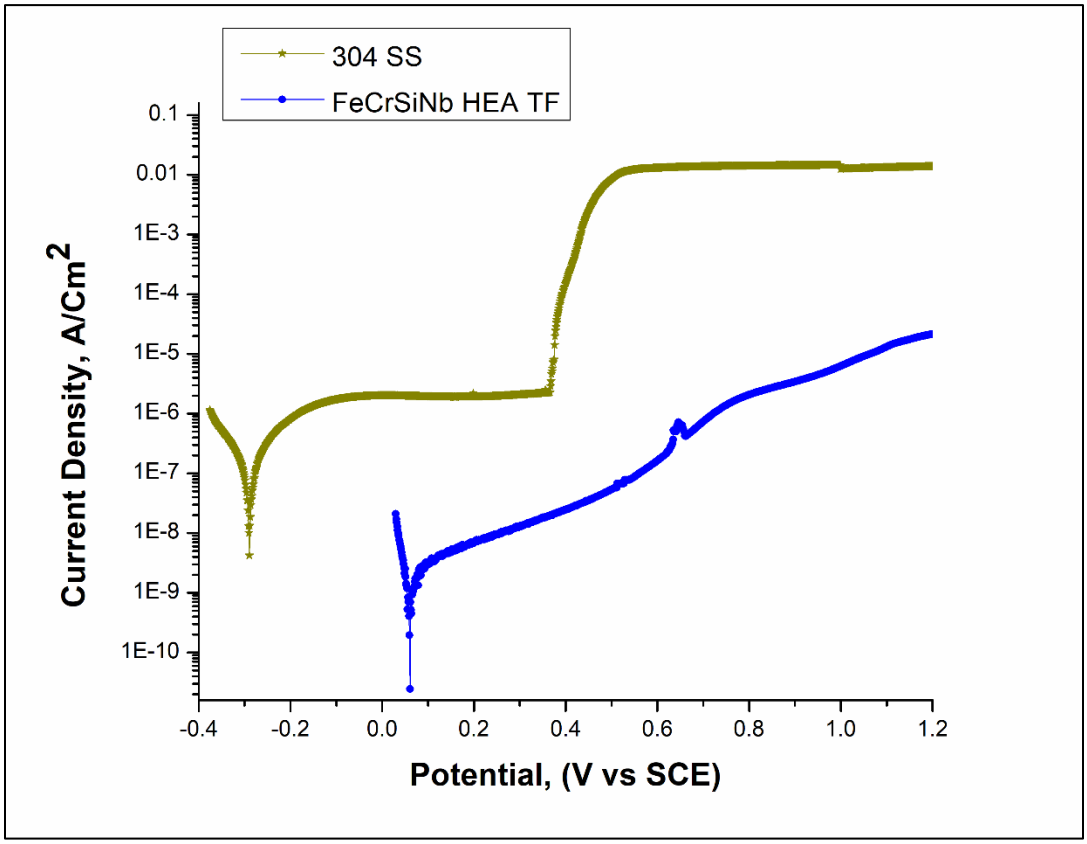

Figure 7: polarisation curves of the amorphous equiatomic FeCrSiNb high entropy alloy thin film and 304 SS in 0.6 M NaCl solution.

Table 1: corrosion parameters of FeCrSiNb HEA thin film and 304 SS in 0.6 M NaCl solution.

Sample ID	i_{corr}, A/Cm^2	E_{corr}, V_{SCE}
FeCrSiNb	8.66*E^{-10}	0.06
304 SS	1.10*E^{-7}	-0.29

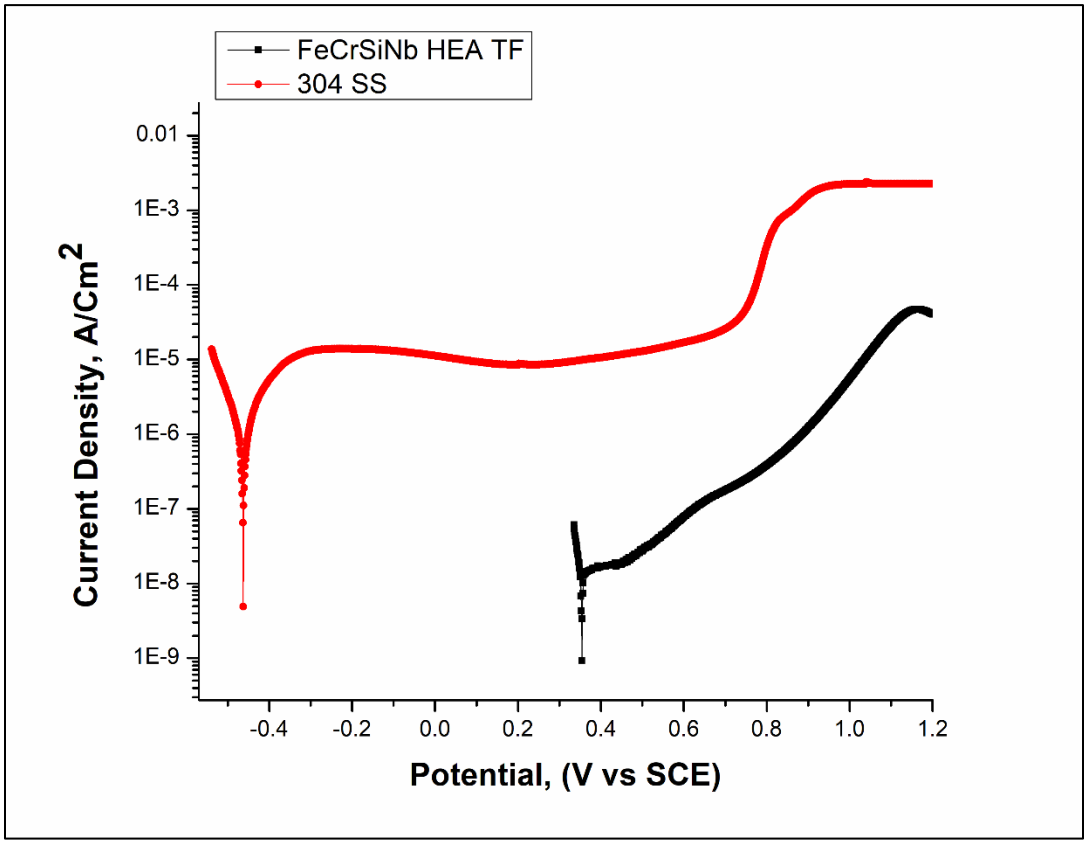

Figure 8: polarisation curves of amorphous equiatomic FeCrSiNb high entropy alloy thin film and 304 SS in 0.6 M H_2SO_4 solution.

Table 2: corrosion parameters of FeCrSiNb HEA thin film and 304 SS in 0.6 M H_2SO_4 solution.

Sample ID	i_{corr}, A/Cm^2	E_{corr}, V_{SCE}
FeCrSiNb	1.22*E^{-8}	0.36
304 SS	4.86*E^{-6}	-0.46

Figure 9 displays a potentiodynamic polarisation curve of the amorphous equiatomic FeCrSiNb high entropy alloy thin film which was carried out in crude oil under conditions of atmospheric pressure and room temperature. The obtained corrosion parameters are listed in table 3.

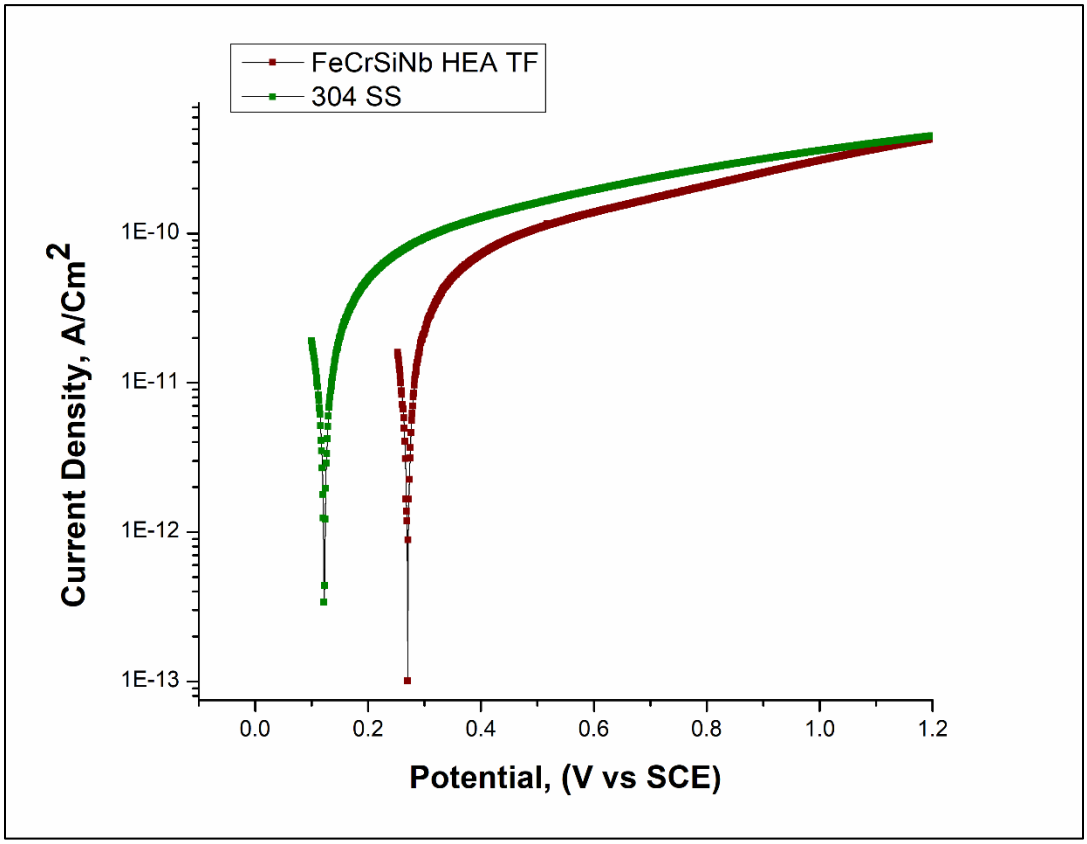

Figure 9: polarisation curves of FeCrSiNb HEA thin film & 304 SS in crude oil.

Table 3: corrosion parameters of FeCrSiNb HEA thin film and 304 SS in crude oil

Sample ID	i_{corr}, A/Cm^2	E_{corr}, V_{SCE}
FeCrSiNb	8.56*E^{-12}	0.27
304 SS	9.91*E^{-12}	0.12

It is well known in electrochemistry when analysing the corrosion performance of a material, that when there is a smaller current density and a higher corrosion potential, the resistance to corrosion is better. In addition, the passivation layer occurs when the corrosion potential shifts to the positive site with continuing the corrosion current density at the same value or a gradually increasing [70, 93, 94].

As it can be seen from the polarisation curve in fig.7 and corrosion parameters of the FeCrSiNb HEA thin film and 304 SS in 0.6 M NaCl solution in table.1, the FeCrSiNb HEA thin film has a corrosion potential of 0.06 V and corrosion current density of $8.66*E^{-10}$ A/Cm^2, comparing to -0.29 V and $1.1*E^{-7}$ A/Cm^2 for 304 SS. From fig.8 and table.2 the corrosion potential of the HEA thin film is 0.36 V and corrosion current density is $1.22*E^{-8}$ A/Cm^2 in 0.6 M H_2SO_4 solution, whereas 304 SS has -0.46 V and $4.86*E^{-6}$ A/Cm^2.

In addition, 304 SS shows a presence of passive layers, then protective oxide failure happens and pitting occurs suddenly in both solutions. In the case of amorphous equiatomic FeCrSiNb HEA thin film, the corrosion current density is increasing slowly, non-exponentially, (where the obvious pitting occurs) and reach to a stable area at around E-5 A/cm^2 of corrosion current density which still a small value at around 1.2 V of corrosion potential in both solutions. Whereas 304 SS at the same value E^{-5} A/cm^2 is clearly in pitting state at around 0.38 V in NaCl and at 0.76 V in H_2SO_4 solutions. This reflects that the corrosion resistance of FeCrSiNb HEA thin film to the corrosion is much higher than 304 SS.

In the case of crude oil test, the FeCrSiNb HEA thin film exhibited a corrosion potential of 0.27 V, higher than that for 304 SS of 0.12 V. The corrosion current density of the amorphous equiatomic FeCrSiNb HEA thin film and 304 SS showed close values with a small advantage for the thin film alloy ($8.56*E^{-12}$, $9.91*E^{-12}$ A/cm^2) respectively. As a result, the amorphous equiatomic FeCrSiNb high entropy alloy thin film has an excellent corrosion resistance nobler than 304 SS in in NaCl, H_2SO_4 solutions and in crude oil.

This can be attributed to several reasons. Generally, the behaviour of high entropy alloys as they have uniform single-phase microstructure with no element separation leads to a good corrosion resistance [74, 95]. Moreover, the cocktail effect of existing elements such as Cr, Si and Nb have the ability to create a passive layer to protect the material from corrosion [43, 82, 96]. The higher corrosion potential (E_{corr}) of amorphous equiatomic FeCrSiNb HEA thin film could be attributed to that high entropy alloys undergo self-passivation at OCP, and forms a

passive protective film as Shi et al. has stated in AlCoCrFeNi HEA [19, 97]. The amorphous structure with the absence of grain boundaries where the corrosion is more likely to happen could enhance the surface resistance to corrosion of the thin film alloy [98]. This has been discussed and proved in earlier work, where the amorphous equiatomic FeCrMnNiC HEA thin film displayed excellent corrosion resistance (E_{corr}=0.07 V, i_{corr}=2.5E^{-10} A/cm^2) in NaCl solution under same conditions [38].

3.3 Mechanical properties:

The hardness measurement of the thin film was carried out by means of nanoindentation. The load was slowly increased from 10 to 50 mN. Loading and unloading was done at fixed time – 20 sec/loading/unloading, dwell period at maximum load was 60 sec, thermal drift correction was done post-indentation for 60 sec.

Hardness measurement with the range of loads allows to account in principle for various effects. At low loads the surface effect, oxide layers for instance, can be identified. It can be seen on Fig. 10 that the penetration curves at low loads are continuously smooth which indicates negligent surface oxide development. The hardness is then can be averaged over measured data. The result showed that amorphous equiatomic HEA thin film has hardness of 15 ± 1.2 GPa. The penetration depth is higher than usually used 1/10th of film thickness but it is rightful as silicon substrate has not so dissimilar to the thin film mechanical values. Fig.11 displays the value of reduced Young's modulus over plastic depth. Smooth decay with plastic penetration depth, as expected, also enforces rightfulness of negligible substrate influence on measured values.

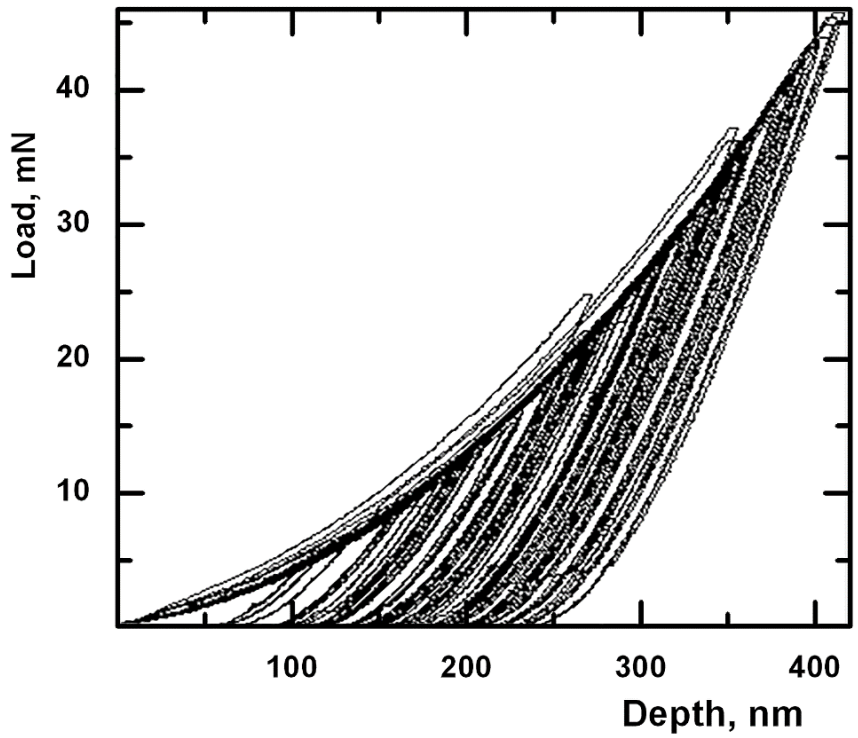

Figure 10. Nanoindentation data set for amorphous equiatomic FeCrSiNb HEA thin film.

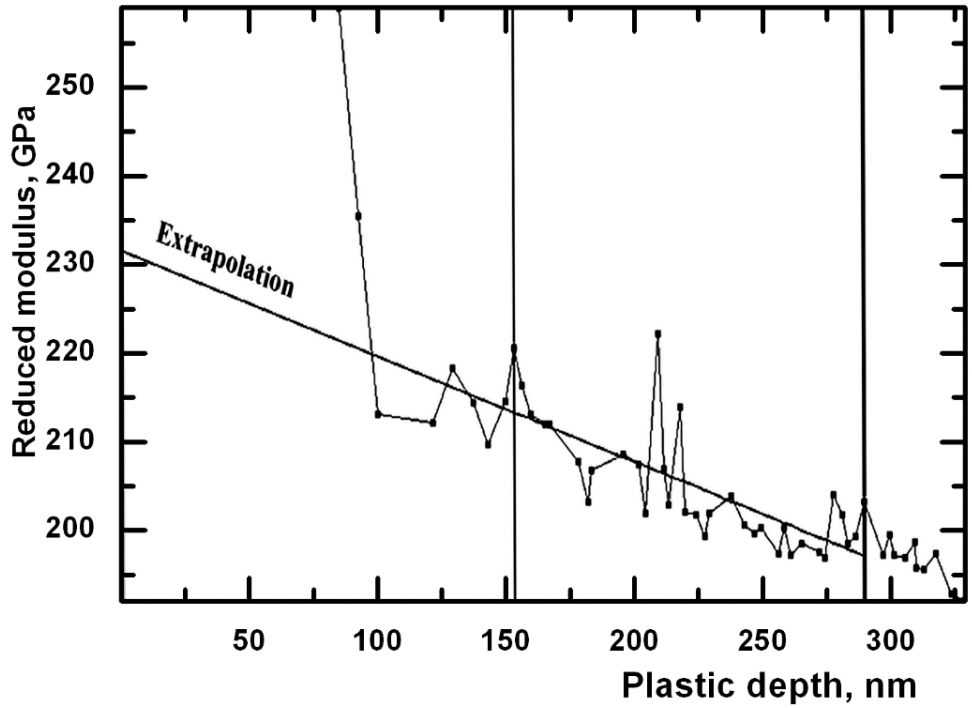

Figure 11. Reduced Young's modulus of amorphous equiatomic FeCrSiNb HEA thin film.

In terms of reduced Young's modulus, the true value should be determined at zero load. This is done by linear extrapolation in accordance with the international standard. In our case the Young's modulus value is at around 229 ± 12 GPa as can be seen on Fig.10.

The obtained mechanical properties in this work were superior to other high entropy thin film alloys. For example, the amorphous equiatomic FeCrSiNb HEA thin film are harder than CoCrFeNi [99] NbTiAlSiZrNx [100] crystalline, and FeCoNiCuVZrAl [101] amorphous high entropy alloy films. The crystalline HETF alloys [99, 100] showed hardness of 8.5 &12.4 GPa and Young's modulus of 161.9 &169 GPa respectively. While the hardness and Young's modulus of amorphous equiatomic HEA thin film were 12 GPa and 166 GPa [101].

These superior properties of high hardness and reduced modulus in this work, are produced due to the effect of the uniform and single-phase structure which led to strengthening of the bonding structure [95]. Furthermore, it could be possible to suggest that the presence of Niobium played a significant role in improving hardness as it was examined in $AlCoCrFeNiNb_x$ High entropy thin film alloy [102].

4. Conclusion:

In conclusion, an amorphous equiatomic FeCrSiNb high entropy alloy thin film was prepared by ion beam sputter deposition. The alloy was confirmed to be equiatomic and amorphous. Corrosion tests were carried out in 0.6 M sodium chloride, sulphuric acid solutions and crude oil using an electrochemical cell. The corrosion parameters proved that the FeCrSiNb HEA thin film is nobler than the 304 SS, as it displayed a higher corrosion potential in NaCl, H_2SO_4 and in crude oil. The amorphous equiatomic FeCrSiNb HEA thin film exhibited a high hardness at 15 ± 1.2 GPa. The Young's modulus value was observed at about 229 ± 12 GPa.

CRediT authorship contribution statement:

Waleed Muftah: conceptualization, methodology, data curation, investigation, formal analysis, writing - original draft, preparation. John Allport: review and editing. Vladimir Vishnyakov: supervision, review & editing.

Declaration of interests:

The authors declare that they have no known competing financial interests or personal relationships that could have appeared to influence the work reported in this paper.

Funding sources:

This research did not receive any specific grant from funding agencies in the public, commercial, or not-for-profit sectors.

References:

1. Telford, M., *The case for bulk metallic glass.* Materials today, 2004. **7**(3): p. 36-43.

2. Wang, D., et al., *Bulk metallic glass formation in the binary Cu–Zr system.* Applied Physics Letters, 2004. **84**(20): p. 4029-4031.

3. Wang, H., et al., *Direct TEM Observation of Phase Separation and Crystallization in Cu 45 Zr 45 Ag 10 Metallic Glass.* Acta Metallurgica Sinica (English Letters), 2016. **29**(6): p. 538-545.

4. Yang, X., et al., *A Novel, Amorphous, Non-equiatomic FeCrAlCuNiSi High-Entropy Alloy with Exceptional Corrosion Resistance and Mechanical Properties.* Acta Metallurgica Sinica (English Letters), 2019: p. 1-7.

5. Okazaki, Y., *2 - Selection of metals for biomedical devices*, in *Metals for Biomedical Devices (Second Edition)*, M. Niinomi, Editor. 2019, Woodhead Publishing. p. 31-94.

6. Kim, Y.C., et al., *Cu-based amorphous alloy composition*. 2006, Google Patents.

7. Smirnova, D. and S. Starikov, *An interatomic potential for simulation of Zr-Nb system.* Computational Materials Science, 2017. **129**: p. 259-272.

8. Ruta, B., E. Pineda, and Z. Evenson, *Relaxation processes and physical aging in metallic glasses.* Journal of Physics: Condensed Matter, 2017. **29**(50): p. 503002.

9. Yeh, J.W., et al., *Nanostructured high-entropy alloys with multiple principal elements: novel alloy design concepts and outcomes.* Advanced Engineering Materials, 2004. **6**(5): p. 299-303.

10. Yeh, J.-W., et al., *Formation of simple crystal structures in Cu-Co-Ni-Cr-Al-Fe-Ti-V alloys with multiprincipal metallic elements.* Metallurgical and Materials Transactions A, 2004. **35**(8): p. 2533-2536.

11. Cantor, B., et al., *Microstructural development in equiatomic multicomponent alloys.* Materials Science and Engineering: A, 2004. **375**: p. 213-218.

12. Huang, P.K., et al., *Multi-principal-element alloys with improved oxidation and wear resistance for thermal spray coating.* Advanced Engineering Materials, 2004. **6**(1-2): p. 74-78.

13. Huang, Y.-S., et al., *Microstructure, hardness, resistivity and thermal stability of sputtered oxide films of AlCoCrCu0. 5NiFe high-entropy alloy.* Materials Science and Engineering: A, 2007. **457**(1-2): p. 77-83.

14. Miracle, D.B. and O.N. Senkov, *A critical review of high entropy alloys and related concepts.* Acta Materialia, 2017. **122**: p. 448-511.

15. Gan, Y., et al., *Multi-layer laser solid forming of Zr65Al7. 5Ni10Cu17. 5 amorphous coating: Microstructure and corrosion resistance.* Optics & Laser Technology, 2015. **69**: p. 17-22.

16. Hsu, C.-Y., et al., *Effect of aluminum content on microstructure and mechanical properties of Al x CoCrFeMo 0.5 Ni high-entropy alloys.* Jom, 2013. **65**(12): p. 1840-1847.

17. Lee, C., et al., *Effect of the aluminium content of AlxCrFe1. 5MnNi0. 5 high-entropy alloys on the corrosion behaviour in aqueous environments.* Corrosion Science, 2008. **50**(7): p. 2053-2060.

18. Lee, C., et al., *Enhancing pitting corrosion resistance of AlxCrFe1. 5MnNi0. 5 high-entropy alloys by anodic treatment in sulfuric acid.* Thin Solid Films, 2008. **517**(3): p. 1301-1305.

19. Shi, Y., et al., *Corrosion of Al xCoCrFeNi high-entropy alloys: Al-content and potential scan-rate dependent pitting behavior.* Corrosion Science, 2017. **119**: p. 33-45.

20. Tung, C.-C., et al., *On the elemental effect of AlCoCrCuFeNi high-entropy alloy system.* Materials letters, 2007. **61**(1): p. 1-5.

21. Xia, S., et al., *Irradiation resistance in Al x CoCrFeNi high entropy alloys.* Jom, 2015. **67**(10): p. 2340-2344.

22. Zhang, F., et al., *Effect of high-energy-density pulse current on solidification microstructure of FeCrNi alloy.* Mater. Sci, 2007. **13**(2): p. 120-122.

23. Zhou, Q., et al., *Corrosion behavior of Hf0. 5Nb0. 5Ta0. 5Ti1. 5Zr refractory high-entropy in aqueous chloride solutions.* Electrochemistry Communications, 2019. **98**: p. 63-68.

24. Jensen, J., et al., *Characterization of the microstructure of the compositionally complex alloy Al1Mo0. 5Nb1Ta0. 5Ti1Zr1.* Scripta Materialia, 2016. **121**: p. 1-4.

25. Qiu, Y., et al., *A lightweight single-phase AlTiVCr compositionally complex alloy.* Acta Materialia, 2017. **123**: p. 115-124.

26. Gorsse, S., J.-P. Couzinié, and D.B. Miracle, *From high-entropy alloys to complex concentrated alloys.* Comptes Rendus Physique, 2018. **19**(8): p. 721-736.

27. Gorsse, S., D.B. Miracle, and O.N. Senkov, *Mapping the world of complex concentrated alloys.* Acta Materialia, 2017. **135**: p. 177-187.

28. Gorsse, S., et al., *Database on the mechanical properties of high entropy alloys and complex concentrated alloys.* Data in brief, 2018. **21**: p. 2664-2678.

29. Muftah, W. and V. Vishnyakov, *Microstructure and properties of FeCrMnNiCx compositionally complex bulk alloys.* Vacuum, 2021: p. 110181.

30. Li, Z., et al., *Metastable high-entropy dual-phase alloys overcome the strength–ductility trade-off.* Nature, 2016. **534**(7606): p. 227-230.

31. Zuo, T.-t., et al., *Processing effects on the magnetic and mechanical properties of FeCoNiAl 0.2 Si 0.2 high entropy alloy.* International Journal of Minerals, Metallurgy, and Materials, 2013. **20**(6): p. 549-555.

32. Senkov, O., et al., *Microstructure and room temperature properties of a high-entropy TaNbHfZrTi alloy.* Journal of alloys and compounds, 2011. **509**(20): p. 6043-6048.

33. Ding, H. and K. Yao, *High entropy Ti20Zr20Cu20Ni20Be20 bulk metallic glass.* Journal of Non-Crystalline Solids, 2013. **364**: p. 9-12.

34. Li, H., et al., *In vitro and in vivo studies on biodegradable CaMgZnSrYb high-entropy bulk metallic glass.* Acta biomaterialia, 2013. **9**(10): p. 8561-8573.

35. Qi, T., et al., *Soft magnetic Fe25Co25Ni25 (B, Si) 25 high entropy bulk metallic glasses.* Intermetallics, 2015. **66**: p. 8-12.

36. Tseng, K., et al., *A light-weight high-entropy alloy Al 20 Be 20 Fe 10 Si 15 Ti 35.* Science China Technological Sciences, 2018. **61**(2): p. 184-188.

37. Yang, X., et al., *A Novel, Amorphous, Non-equiatomic FeCrAlCuNiSi High-Entropy Alloy with Exceptional Corrosion Resistance and Mechanical Properties.* Acta Metallurgica Sinica (English Letters), 2020. **33**(8): p. 1057-1063.

38. Muftah, W., N. Patmore, and V. Vishnyakov, *Demanding applications in harsh environment–FeCrMnNiC amorphous equiatomic alloy thin film.* Materials Science and Technology, 2020. **36**(12): p. 1301-1307.

39. Kucza, W., et al., *Studies of "sluggish diffusion" effect in Co-Cr-Fe-Mn-Ni, Co-Cr-Fe-Ni and Co-Fe-Mn-Ni high entropy alloys; determination of tracer diffusivities by combinatorial approach.* Journal of Alloys and Compounds, 2018. **731**: p. 920-928.

40. Pickering, E. and N. Jones, *High-entropy alloys: a critical assessment of their founding principles and future prospects.* International Materials Reviews, 2016. **61**(3): p. 183-202.

41. Tsai, K.-Y., M.-H. Tsai, and J.-W. Yeh, *Sluggish diffusion in Co–Cr–Fe–Mn–Ni high-entropy alloys.* Acta Materialia, 2013. **61**(13): p. 4887-4897.

42. Miracle, D.B., *High-entropy alloys: A current evaluation of founding ideas and core effects and exploring "nonlinear alloys".* Jom, 2017. **69**(11): p. 2130-2136.

43. Jien-Wei, Y., *Recent progress in high entropy alloys.* Ann. Chim. Sci. Mat, 2006. **31**(6): p. 633-648.

44. Macdonald, B., et al., *Recent progress in high entropy alloy research.* JOM, 2017. **69**(10): p. 2024-2031.

45. Schuh, B., et al., *Mechanical properties, microstructure and thermal stability of a nanocrystalline CoCrFeMnNi high-entropy alloy after severe plastic deformation.* Acta Materialia, 2015. **96**: p. 258-268.

46. Shivam, V., V. Sanjana, and N.K. Mukhopadhyay, *Phase Evolution and Thermal Stability of Mechanically Alloyed AlCrFeCoNiZn High-Entropy Alloy.* Transactions of the Indian Institute of Metals, 2020. **73**(3): p. 821-830.

47. Sriharitha, R., B.S. Murty, and R.S. Kottada, *Alloying, thermal stability and strengthening in spark plasma sintered AlxCoCrCuFeNi high entropy alloys.* Journal of Alloys and Compounds, 2014. **583**: p. 419-426.

48. Heczel, A., et al., *Defect structure and hardness in nanocrystalline CoCrFeMnNi High-Entropy Alloy processed by High-Pressure Torsion.* Journal of Alloys and Compounds, 2017. **711**: p. 143-154.

49. Moon, J., et al., *Microstructure and Mechanical Properties of High-Entropy Alloy Co20Cr26Fe20Mn20Ni14 Processed by High-Pressure Torsion at 77 K and 300 K.* Scientific Reports, 2018. **8**(1): p. 11074.

50. Youssef, K.M., et al., *A Novel Low-Density, High-Hardness, High-entropy Alloy with Close-packed Single-phase Nanocrystalline Structures.* Materials Research Letters, 2015. **3**(2): p. 95-99.

51. Zhang, T., et al., *Microstructure and mechanical properties of FexCoCrNiMn high-entropy alloys.* Journal of Materials Science & Technology, 2019. **35**(10): p. 2331-2335.

52. Senkov, O.N., et al., *Mechanical properties of Nb25Mo25Ta25W25 and V20Nb20Mo20Ta20W20 refractory high entropy alloys.* Intermetallics, 2011. **19**(5): p. 698-706.

53. Wang, C., et al., *Hardness and strength enhancements of CoCrFeMnNi high-entropy alloy with Nd doping.* Materials Science and Engineering: A, 2019. **764**: p. 138192.

54. Sadeghilaridjani, M., et al., *Ion irradiation response and mechanical behavior of reduced activity high entropy alloy.* Journal of Nuclear Materials, 2020. **529**: p. 151955.

55. Xia, S., et al., *Phase stability and microstructures of high entropy alloys ion irradiated to high doses.* Journal of Nuclear Materials, 2016. **480**: p. 100-108.

56. Kumar, N.K., et al., *Microstructural stability and mechanical behavior of FeNiMnCr high entropy alloy under ion irradiation.* Acta Materialia, 2016. **113**: p. 230-244.

57. Chuang, M.-H., et al., *Microstructure and wear behavior of AlxCo1. 5CrFeNi1. 5Tiy high-entropy alloys.* Acta Materialia, 2011. **59**(16): p. 6308-6317.

58. Löbel, M., T. Lindner, and T. Lampke, *Enhanced Wear Behaviour of Spark Plasma Sintered AlCoCrFeNiTi High-Entropy Alloy Composites.* Materials, 2018. **11**(11): p. 2225.

59. Chen, P., et al., *Fatigue behavior of high-entropy alloys: A review.* Science China Technological Sciences, 2018. **61**(2): p. 168-178.

60. Kashaev, N., et al., *Fatigue behaviour of a laser beam welded CoCrFeNiMn-type high entropy alloy.* Materials Science and Engineering: A, 2019. **766**: p. 138358.

61. Lee, G.T., et al., *Effect of Microstructural Features on the High-Cycle Fatigue Behavior of CoCrFeMnNi High-Entropy Alloys Deformed at Room and Cryogenic Temperatures.* Metals and Materials International, 2020.

62. Holcomb, G.R., J. Tylczak, and C. Carney, *Oxidation of CoCrFeMnNi High Entropy Alloys.* JOM, 2015. **67**(10): p. 2326-2339.

63. Müller, F., et al., *On the oxidation mechanism of refractory high entropy alloys.* Corrosion Science, 2019. **159**: p. 108161.

64. Shajahan, S., et al., *Oxidation study of CoCrCuFeNiSix high entropy alloys.* Materials Research Express, 2020. **7**(1): p. 016532.

65. Ayyagari, A., et al., *Corrosion, erosion and wear behavior of complex concentrated alloys: a review.* Metals, 2018. **8**(8): p. 603.

66. Qiu, X.-w., et al., *Corrosion performance of Al2CrFeCoxCuNiTi high-entropy alloy coatings in acid liquids.* Journal of Alloys and Compounds, 2017. **708**: p. 353-357.

67. Qiu, Y., et al., *Corrosion characteristics of high entropy alloys.* Materials Science and Technology, 2015. **31**(10): p. 1235-1243.

68. Qiu, Y., et al., *Corrosion of high entropy alloys.* npj Materials degradation, 2017. **1**(1): p. 1-18.

69. Hsu, Y.-J., W.-C. Chiang, and J.-K. Wu, *Corrosion behavior of FeCoNiCrCux high-entropy alloys in 3.5% sodium chloride solution.* Materials Chemistry and Physics, 2005. **92**(1): p. 112-117.

70. Kao, Y.-F., et al., *Electrochemical passive properties of AlxCoCrFeNi (x=0, 0.25, 0.50, 1.00) alloys in sulfuric acids.* Corrosion Science, 2010. **52**(3): p. 1026-1034.

71. Wong, S.-K., et al., *Microstructures and properties of Al0. 3CoCrFeNiMnx high-entropy alloys.* Materials Chemistry and Physics, 2018. **210**: p. 146-151.

72. Chou, Y., J. Yeh, and H. Shih, *The effect of molybdenum on the corrosion behaviour of the high-entropy alloys Co1. 5CrFeNi1. 5Ti0. 5Mox in aqueous environments.* Corrosion Science, 2010. **52**(8): p. 2571-2581.

73. Tang, Z., et al., *Alloying and processing effects on the aqueous corrosion behavior of high-entropy alloys.* Entropy, 2014. **16**(2): p. 895-911.

74. Shi, Y., B. Yang, and P. Liaw, *Corrosion-resistant high-entropy alloys: A review.* Metals, 2017. **7**(2): p. 43.

75. Zhang, S., et al., *Laser surface alloying of FeCoCrAlNi high-entropy alloy on 304 stainless steel to enhance corrosion and cavitation erosion resistance.* Optics & Laser Technology, 2016. **84**: p. 23-31.

76. Chen, S., et al., *Tribo-corrosion behavior of VAlTiCrCu high-entropy alloy film.* Materials Characterization, 2019. **157**: p. 109887.

77. Malinovskis, P., et al., *Synthesis and characterization of multicomponent (CrNbTaTiW) C films for increased hardness and corrosion resistance.* Materials & Design, 2018. **149**: p. 51-62.

78. Wang, H.-d., et al., *Microstructure and corrosion behaviour of AlCoFeNiTiZr high-entropy alloy films.* Surface Engineering, 2020. **36**(1): p. 78-85.

79. Zeng, Q. and Y. Xu, *A comparative study on the tribocorrosion behaviors of AlFeCrNiMo high entropy alloy coatings and 304 stainless steel.* Materials Today Communications, 2020: p. 101261.

80. Zhao, S., et al., *Microstructure and chloride corrosion property of nanocrystalline AlTiCrNiTa high entropy alloy coating on X80 pipeline steel.* Surface and Coatings Technology, 2019. **375**: p. 215-220.

81. Qiu, X., Y. Zhang, and C. Liu, *Effect of Ti content on structure and properties of Al2CrFeNiCoCuTix high-entropy alloy coatings.* Journal of alloys and compounds, 2014. **585**: p. 282-286.

82. Wang, W., et al., *Microstructure and Corrosion behavior of (CoCrFeNi) 95Nb5 high-entropy alloy coating fabricated by plasma spraying.* Materials, 2019. **12**(5): p. 694.

83. Cheng, J., et al., *Formation and mechanical properties of CoNiCuFeCr high-entropy alloys coatings prepared by plasma transferred arc cladding process.* Plasma Chemistry and Plasma Processing, 2013. **33**(5): p. 979-992.

84. Tian, Y., et al., *Microstructure and corrosion property of CrMnFeCoNi high entropy alloy coating on Q235 substrate via mechanical alloying method.* Surfaces and Interfaces, 2019. **15**: p. 135-140.

85. Craig, B.D. and L. Smith, *Corrosion Resistant Alloys (CRAs) in the oil and gas industry.* Nickel Institute Technical Series, 2011. **1**: p. 0073.

86. Lipp, W. and S. Shafer, *The future of corrosion resistant steels and alloys in the oil and gas industry.* Stainless steel world, 2013. **25**: p. 29-32.

87. Popoola, L.T., et al., *Corrosion problems during oil and gas production and its mitigation.* International Journal of Industrial Chemistry, 2013. **4**(1): p. 35.

88. Vishnyakov, V., et al., *Ion sputter-deposition and in-air crystallisation of Cr2AlC films.* Vacuum, 2014. **100**: p. 61-65.

89. Vishnyakov, V., et al., *Amorphous Boron containing silicon carbo-nitrides created by ion sputtering.* Surface and Coatings Technology, 2011. **206**(1): p. 149-154.

90. Guo, S., et al., *More than entropy in high-entropy alloys: Forming solid solutions or amorphous phase.* Intermetallics, 2013. **41**: p. 96-103.

91. Li, W., P. Liu, and P.K. Liaw, *Microstructures and properties of high-entropy alloy films and coatings: a review.* Materials Research Letters, 2018. **6**(4): p. 199-229.

92. Braeckman, B. and D. Depla, *Structure formation and properties of sputter deposited Nbx-CoCrCuFeNi high entropy alloy thin films.* Journal of Alloys and Compounds, 2015. **646**: p. 810-815.

93. Pletcher, D. and F.C. Walsh, *Industrial electrochemistry*. 2012: Springer Science & Business Media.

94. Shun, T.-T., C.-H. Hung, and C.-F. Lee, *The effects of secondary elemental Mo or Ti addition in Al0. 3CoCrFeNi high-entropy alloy on age hardening at 700 C.* Journal of Alloys and Compounds, 2010. **495**(1): p. 55-58.

95. Zhang, Y., et al., *Microstructures and properties of high-entropy alloys.* Progress in Materials Science, 2014. **61**: p. 1-93.

96. Nene, S., et al., *Corrosion-resistant high entropy alloy with high strength and ductility.* Scripta Materialia, 2019. **166**: p. 168-172.

97. Shi, Y., et al., *In-situ electrochemical-AFM study of localized corrosion of AlxCoCrFeNi high-entropy alloys in chloride solution.* Applied Surface Science, 2018. **439**: p. 533-544.

98. Li, R., et al., *Structure and corrosion resistance properties of Ni–Fe–B–Si–Nb amorphous composite coatings fabricated by laser processing.* Journal of alloys and compounds, 2013. **580**: p. 327-331.

99. Huo, W., et al., *Ultrahigh hardness and high electrical resistivity in nano-twinned, nanocrystalline high-entropy alloy films.* Applied Surface Science, 2018. **439**: p. 222-225.

100. Xing, Q., et al., *Mechanical properties and corrosion resistance of NbTiAlSiZrNx high-entropy films prepared by RF magnetron sputtering.* Entropy, 2019. **21**(4): p. 396.

101. Liu, L., et al., *Dense and smooth amorphous films of multicomponent FeCoNiCuVZrAl high-entropy alloy deposited by direct current magnetron sputtering.* Materials & Design, 2013. **46**: p. 675-679.

102. Jiang, H., et al., *Synthesis and characterization of AlCoCrFeNiNbx high-entropy alloy coatings by laser cladding.* Crystals, 2019. **9**(1): p. 56.